

Bistability of moving and self-pinned fronts of supercritical localized convection structures

D. JUNG and M. LÜCKE

Institut für Theoretische Physik, Universität des Saarlandes - Postfach 151150, D-66041 Saarbrücken, Germany

received 6 March 2007; accepted in final form 6 August 2007

published online 31 August 2007

PACS 47.20.-k – Flow instabilities

PACS 47.54.-r – Pattern selection; pattern formation

PACS 47.20.Ky – Nonlinearity, bifurcation, and symmetry breaking

Abstract – Localized stationary structures that are embedded at supercritical driving in a convectively unstable homogeneous surrounding are investigated by numerical simulations of convection in binary fluid mixtures with weakly negative separation ratios. Bistability of pinned and moving fronts is found in a finite driving interval. The pinning mechanism and the different transition scenarios between pinned and moving fronts at the two ends of the pinning interval is identified to be strongly influenced by the concentration field. Its advective lateral redistribution acting on a sub-wavelength scale allows to explain the observed behavior.

Copyright © EPLA, 2007

Self-organized structures appear in a wide variety of nonlinear driven systems [1]. For example, a homogeneous state that is stable at small driving undergoes a symmetry-breaking instability and a new spatially extended structured solution of the underlying equations bifurcates out of the homogeneous one. The behavior of fronts that connect and separate in real space such a structured state and the homogeneous one has been attracting much research activities [2].

Forwards bifurcating structures are intuitively expected to expand at supercritical control parameters thereby replacing the unstable homogeneous state [2,3]. The case of backwards bifurcating structured solutions is more complicated. In variational models like the cubic quintic Ginzburg-Landau equation with amplitude dynamics driven by potential gradients front motion into or out of the homogeneous state and front pinning [4,5] is largely governed by the control parameter's location relative to the Maxwell point where the potential minima of the two states are at the same height such that for large driving the structured state expands. However, in strongly nonlinear real systems the front dynamics can be more complicated and does not fit into this picture.

We investigate here a situation where broad localized structures of stationary patterns are stably embedded at *supercritical* driving in a homogeneous surrounding that is linearly unstable. We elucidate the physics of the pinning mechanism that prevents the fronts of such localized states to move into the homogeneous state. We show that and

why in a finite range of control parameters bistability occurs between such self-pinned fronts and those which can invade the homogeneous state.

System. This behavior can be seen in horizontal layers of binary miscible fluids heated from below. The structural and dynamical richness of convection patterns in this system [1,6] relative to one-component fluids is ultimately due to the Soret effect. It partially separates the two components in a temperature gradient. The resulting concentration variations are advected by the flow and then feed back by changing the buoyancy force that drives the flow itself. The strength of the Soret effect is measured by the separation ratio ψ . We consider here mixtures like, *e.g.*, ethanol-water for which $\psi < 0$ so that the lighter ethanol is thermophobic: it tends to migrate into cooler regions, say, close to the top boundary and thereby weakens the buoyancy. Thus, the quiescent conductive state is stabilized by the Soret-induced vertical ethanol concentration profile of slope $\partial C_{cond}/\partial z = -\psi$ (see footnote ¹).

¹In this paper lengths are scaled by the layer thickness d and velocities by κ/d with κ denoting the heat diffusion constant. Concentration is reduced by $\frac{\alpha}{\beta}\Delta T$. Here ΔT is the vertical temperature difference across the layer and α and β are thermal and solutal expansion coefficients, respectively, of the total mass density. Furthermore, reduced Rayleigh numbers $r = R/R_c^0$ are introduced with R_c^0 being the critical one for onset of pure fluid convection. The values for the kinematic viscosity $\nu = 10\kappa$ and the concentration diffusion constant $D = 0.01\kappa$ were chosen to be representative of ethanol-water mixtures.

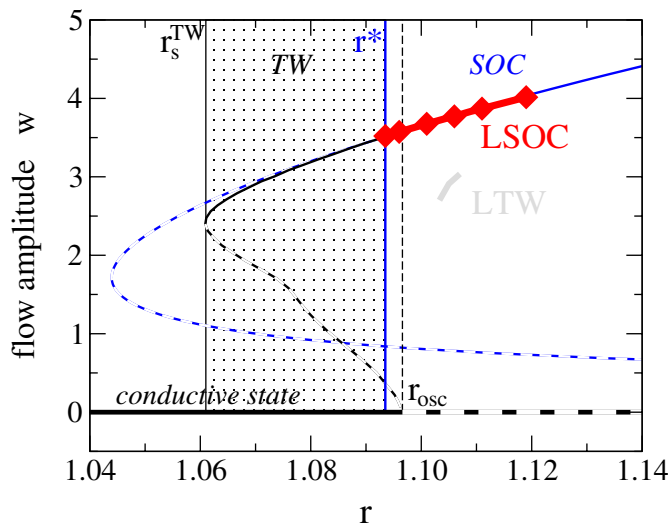


Fig. 1: (Color online) Representative bifurcation diagrams of the maximal vertical velocity w vs. reduced Rayleigh number r for spatially extended TW and SOC solutions with wave number $k = \pi$, for LSOC, and for short LTW pulses [7]. Full (dashed) lines refer to stable (unstable) solutions obtained for $\psi = -0.08$. SOC and LSOC exist stably only in the region above r^* where the drift instability mechanism to TW oscillations is suppressed by sufficient advective homogenization of the concentration field. The existence region of large-amplitude TWs between the saddle r_s^{TW} and r^* is dotted for reference in later figures.

The Soret effect not only shifts the onset of convection to (reduced) Rayleigh numbers $r > 1$ and makes the bifurcation to extended convection backwards, but it also generates via a Hopf bifurcation at r_{osc} oscillatory convection, *e.g.*, in the form of spatially extended traveling waves (TWs). The bifurcation diagrams in fig. 1 and the phase diagram of fig. 2 provide an overview over the convective solutions² in the vicinity of r_{osc} (disregarding, however, standing waves [9]). Note that, compared to pure fluids it is the concentration field (and its interplay with the other fields) that causes all the new convection phenomena in mixtures.

Except for narrow boundary layers and a lateral concentration redistribution in localized states—that is important for their explanation and that is discussed further below—large-amplitude convection in mixtures resembles that of homogeneous fluids: with increasing flow amplitude the associated advective mixing reduces more and more the Soret-generated concentration differences being largest in the quiescent fluid. For example, upon increasing the heating beyond r^* in figs. 1 and 2 this advective reduction of concentration differences reduces the restoring forces that drive TW oscillations to zero. Then,

²We have solved the full hydrodynamic field equations [6] in a vertical cross-section perpendicular to the roll axes with a finite difference method for $\psi = -0.05$ and -0.08 . These simulations are adapted to convection in narrow annular systems [8] with a circumference of, say, 80.

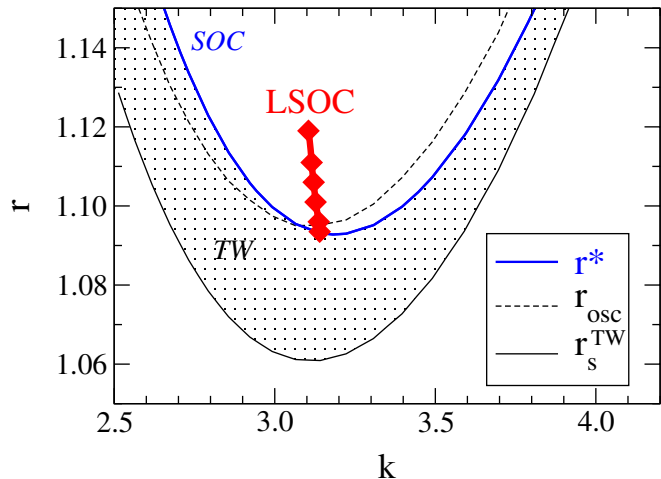


Fig. 2: (Color online) Phase diagram of convective states in the k - r -plane for $\psi = -0.08$. All long LSOCs (thick red line with diamonds) that we found to be stable for this separation ratio are characterized by a uniquely selected bulk wave number. A nonlinear extended SOC in the k - r region below the drift instability line r^* loses its stability there to a nonlinear TW. The latter exists down to the saddle line r_s^{TW} . The quiescent state is stable below the oscillatory bifurcation threshold r_{osc} . Bistability between LSOC and the basic state occurs only in the narrow interval for which $r^* < r_{osc}$.

without the competing existence of extended TWs above r^* stationary overturning convection (SOC) is stable there. However, below r^* SOC is drift-unstable to TW oscillations.

Supercritical LSOC. The stable localized SOC (LSOC) solutions shown in figs. 1 and 2 appear in the driving region where the quiescent state is unstable (except for a narrow interval when $r^* < r_{osc}$) and where the extended SOC are stable, *c.f.* the discussion below for details. LSOC have been found in simulations of ${}^3\text{He}$ - ${}^4\text{He}$ mixtures [10] (where they were called “convectons”) and ethanol-water mixtures [11] and they seem to have been seen in experiments with ethanol-water mixtures [12]. Batiste *et al.* [10,11] have revealed their snake-like structure of alternating stable and unstable solution branches stacked upon each other in Nusselt number vs. Rayleigh number bifurcation diagrams and thus the multistability of LSOC solutions with different numbers of convection rolls for the same parameters.

In contrast to localized TWs (LTWs) [13], *long* LSOCs can be interpreted due to the vanishing phase and group velocity of the underlying pattern as pairs of effectively noninteracting stationary fronts between SOC and quiescent fluid. Our investigation reveals the role that the lateral concentration distribution plays for stationary and moving SOC-fronts and for the robust existence of LSOCs.

Differences to pinning scenario of subcritical fronts. The pinning of fronts that connect a *subcritically stable* homogeneous state to a structured one has been explained [4]

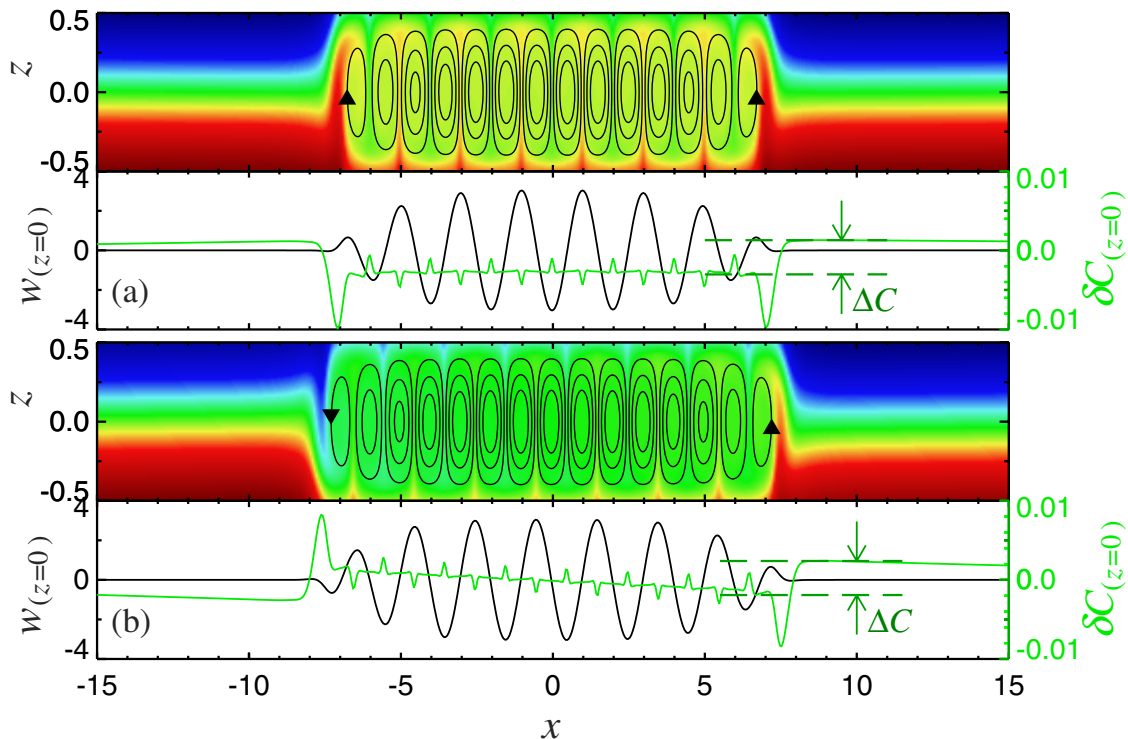


Fig. 3: Even LSOC of 14 rolls (a) and odd LSOC of 15 rolls (b) both existing stably for $r = 1.071$, $\psi = -0.05$. Top plots show in each case color-coded concentration deviations, $\delta C(x, z)$, from the global mean together with streamlines of the velocity field in an x - z cross-section perpendicular to the roll axes: regions with maximal positive (negative) δC are blue (red). Green refers to the mean value $\delta C = 0$. Arrows indicate turning directions of the outermost rolls. Lower plots show the lateral profiles of δC and of the vertical velocity w at mid height $z = 0$. Both LSOC were obtained in a computational domain of length $\Gamma = 80$ with laterally periodic boundary conditions.

within the framework of amplitude equations in the vicinity of the Maxwell point by an interaction between the front's large scale amplitude variation and the underlying periodic pattern at the scale of a wavelength [5]. Then the velocities of fronts moving into or out of the stable homogeneous state grow continuously from zero proportional to the square root of the distance from the unpinning transitions [14–16]. Here, however, a stabilizing mechanism is operating that can prevent SOC fronts from invading the *unstable* conductive state. Also the transitions between pinned and unpinned fronts are different. In particular the transition to pattern expanding fronts is hysteretic such that bistability between pinned and unpinned fronts occurs. We explain this behavior in terms of the characteristics of sub-wavelength scaled, almost step-like variations of the concentration field that are generated advectively across the fronts.

Conditions for robust stationary supercritical fronts.

The long LSOCs which we have examined occur with an uniquely selected bulk wave number in a parameter regime where nonlinear TWs do not exist, where the quiescent fluid is only convectively, *i.e.*, not absolutely unstable [11] to localized TW perturbations [17], and where it is linearly stable against the growth of stationary convection. These

conditions do not explain the ultimate physical mechanism for the stabilization of LSOCs but they are favorable for their robust existence: i) Above r^* the drift-decay channel to a TW is not available for the wave-number-selected LSOC. ii) Localized TW *perturbations* that can grow out of the quiescent fluid are advected away by their fast group velocity in the convectively unstable regime and/or are absorbed by the LSOC. iii) Finally, and most importantly, the conductive state is stable against growth of SOC rolls: The (local) buoyancy and flow has to be sufficiently large to induce growth of a SOC roll out of the quiescent fluid—the lower dashed SOC branch in fig. 1 is a separatrix between decay and growth of a roll. Consequently the expansion of LSOCs into the quiescent fluid at the front edges is governed by a delicate nonlinear buoyancy balance that might contain the effects discussed in [4,5]. In binary mixtures it is the concentration field that determines the balance.

Concentration redistribution. Symmetry under lateral reflection of the system allows to classify LSOCs into even and odd states [10]. Figure 3 shows the concentration and velocity fields of an even and an odd example that are both stable at the same parameters, the particular realization being decided by initial conditions. Within the

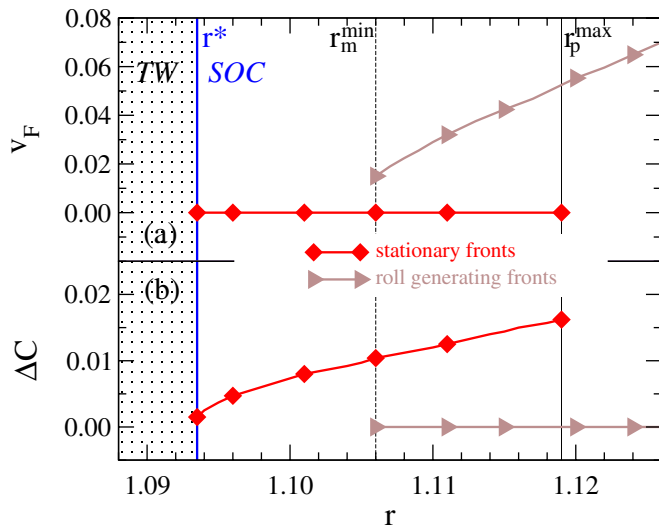


Fig. 4: (Color online) Bifurcation diagrams of velocity v_F (a) and concentration step ΔC (b) of fronts between long LSOCs and the unstable quiescent fluid for $\psi = -0.08$. Lines with diamonds (triangles) denote pinned (moving) fronts. For better visibility only a few symbols are shown as in previous figures. See text for a discussion of the bistability of and hysteresis between pinned and moving fronts.

central SOC-like part there are only small δC -differences. They are determined by an interplay between the vertical feeding out of the Soret dominated boundary layers near the plates into counter rotating roll pairs in the bulk, by the bulk advective mixing within the rolls, and by advection from the rolls at each end of the LSOC. The unpaired outermost roll under each front couples strongly to the concentration in the adjacent conductive state and in the boundary layers.

Thus, in the even LSOC of fig. 3(a) the turning directions of the rolls at both ends are such as to suck in predominantly low concentrated “red” fluid from the conductive side. This generates red upwards pointing plumes there. They cause the negative δC peak in the green curve. Similarly the left turning roll at the left end of the odd LSOC of fig. 3(b) generates a downwards pointing “blue” plume of high concentration. In this way the outermost rolls transport out of the quiescent fluid strongly negative δC via the red plumes laterally into the LSOC bulk and strongly positive δC via the blue plumes. Thereby δC is increased on the convective side of a front with a blue plume and decreased on its conductive side and vice versa for the front with a red plume. Note that the plume-like sub-wavelength variations of the concentration field reflect its *strongly* nonlinear, *i.e.*, advection-dominated behavior that can not be captured by weakly nonlinear analysis. The smooth variation of the velocity field, on the other hand, reflects the weakly nonlinear nature of the momentum balance.

So each outermost roll maintains by shuffling δC out of the quiescent fluid into the convective bulk a characteristic

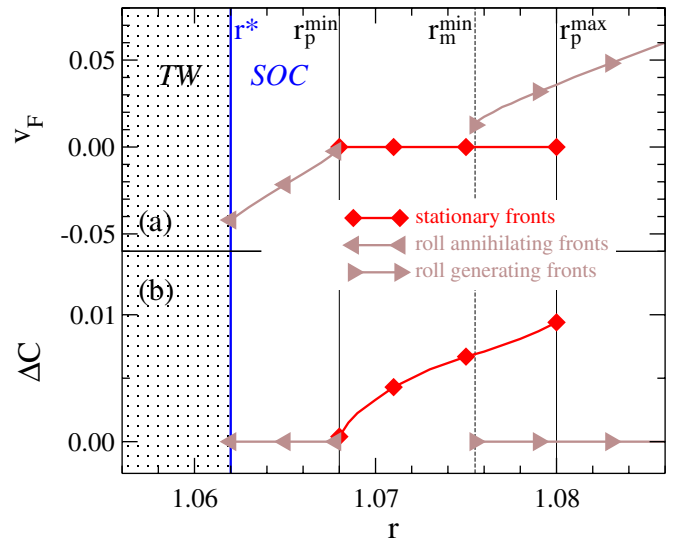


Fig. 5: (Color online) Same as fig. 4, however, for smaller Soret coupling ($\psi = -0.05$) and thus smaller pinning by the concentration step. For better visibility only a few symbols are shown. See text for further details.

difference between the mean concentration levels on the two sides of the front that is indicated in fig. 3 by ΔC . This enforced concentration step of size ΔC acts somewhat like a boundary condition on its conduction and convection side. In LSOCs that are even under lateral reflection as in fig. 3(a) the end rolls turn in opposite direction and thus cause the same concentration steps. The rolls at the ends of odd LSOCs turning in the same direction, on the other hand, generate concentration steps of opposite sign. Within the LSOC the two step conditions are diffusively connected to each other, *i.e.*, with a laterally constant profile as in fig. 3(a) or a linearly varying one as in fig. 3(b).

Symmetry considerations. Due to the $z \leftrightarrow -z$ up-down flow symmetry of SOC solutions of the Oberbeck-Boussinesq equations a particular realization of LSOCs and of (single) front states is symmetry related to the one in which the turning directions of all rolls are reverted. Thus, *e.g.*, the plumes at the fronts in fig. 3(a) would be downwards directed and blue. Moreover, fronts like those in fig. 3(b) are symmetry related to each other. We therefore treat them in the following as identical.

Concentration step and front pinning. The lateral concentration step across stationary fronts grows with increasing r as shown in figs. 4 and 5. This short-scale concentration variation creates a mean lateral buoyancy difference between the two sides of the front. In a globally quiescent state such a buoyancy step would induce convection rolls with a vorticity the sign of which is determined by the sign of the buoyancy step. In the pinned states this vorticity is opposite to the vorticity of the roll that would have to be nucleated in order to expand convection into the conduction state. Consider first the right fronts in fig. 3. Compared to their convective sides the positive offset of

ΔC provides an increased upwards pointing force ahead of the front that prohibits the downflow there that a next roll adjacent to the presently last one would have to realize. Instead, downflow is realized predominantly on the convective side of the front being favored there by the lower C . Because of this redistribution of concentration and the resulting force imbalance (if it is strong enough) no further roll grows and the front is pinned. The same hindering of downwards flow on the conductive side occurs for the left front of fig. 3a. Now consider the left front in fig. 3b. In order to advance to the left into the quiescent fluid a right turning roll would have to be created, *i.e.*, an upflow one roll diameter to the left of the current front position. But there the extra buoyancy force due to the negative offset of C on the conductive side is directed downwards, thus, hindering upflow there. This pinning mechanism differs from the self-trapping of wave packets [18] that was considered in ref. [10]: a finite group velocity of the underlying pattern that is absent here is an essential ingredient in the self-trapping approach to modelling lateral redistribution of solutal buoyancy [13]. Furthermore, the large-scale amplitude formulation does not seem to be adequate to include effects on a sub-wavelength scale seen here.

When the thermal contribution to the buoyancy becomes sufficiently large with increasing r to overcome the solutal pinning force the fronts are no longer locked and convection can expand into the quiescent fluid. This unpinning transition at r_p^{max} is first order with jumps to $\Delta C = 0$ and to a nonzero front velocity v_F .

For moving fronts the turning directions of respective added (or removed) rolls change periodically and with it their concentration shuffling between the conductive and convective sides of the front. Thus, with the vertically antisymmetric solutal profile $C_{cond}(z)$ of the quiescent fluid $C(z=0)$ averages temporally to zero at the moving front so that ΔC vanishes.

Bistability. Roll-generating moving fronts and stationary pinned fronts are bistable solutions in the hysteresis interval $r_m^{min} < r < r_p^{max}$. Both types differ there by the magnitude of ΔC , cf. figs. 4 and 5 with ΔC being nonzero only for stationary fronts. We consider ΔC to be an adequate measure for the solutal part of the stationary fronts pinning effect. This is based among others on the following three observations: i) Investigating front transitions in the coexistence regime we have found evolutions towards the attractors of moving or pinned front solutions depending on whether the initial state's ΔC was small or large, respectively. So the competition between the two front attractors in the bistable interval is decided by the magnitude of ΔC . ii) ΔC —and with it the solutal pinning force—at the stationary fronts of an odd LSOC is always smaller than at the fronts of an even LSOC for the same r , cf. fig. 3. This explains the observation [11] that the upper existence limit r_p^{max} of odd LSOCs lies below the one of even LSOCs. Both limits will converge however in the front limit, *i.e.*, for very large roll numbers. iii) Approaching

the lower existence limit of LSOCs the concentration step at the fronts decreases with decreasing r . For the small Soret coupling of fig. 5 it goes in fact to zero. Then, a roll annihilating front gets unpinned and conduction invades convection.

Note that (within our resolution) the speed of these fronts does not vary as a square root but rather linearly with the distance from the lower continuous unpinning transition at r_p^{min} . This might indicate that also here the moving front solution branch is in fact disconnected from the pinned one. In fig. 4, however, the Soret effect and with it ΔC is so large that the latter does not reach zero at a driving above r^* . Instead, the drift instability to TWs at r^* preempts the unpinning to a roll annihilating front—here, LSOCs cease to exist at r^* before ΔC has dropped to zero.

Conclusion. Simulations of supercritical stationary localized convection structures in binary mixtures have revealed a new bifurcation scenario with bistability between moving and pinned fronts. The buoyancy change resulting from a self-advected concentration distribution with its sub-wavelength scaled step across the LSOC fronts prevents their expansion into the unstable quiescent fluid within a finite pinning interval of r . Furthermore, it is the concentration step which is responsible for the bistability because moving fronts do not show such a step: with rolls having at the moving front interface temporally alternating turning directions the advective concentration transfer between the conductive and convective sides of the front periodically reverses and thus averages to zero. A first-order transition to structure-expanding front motion marks the upper end of the pinning interval, *i.e.*, of the existence range of long LSOC. Its lower end at smaller supercritical r is marked either by a transition to structure-reducing front motion or by a drift instability to TWs.

We expect similar pinning mechanisms in all systems where the (advective) transport of a slowly diffusing field influences the effective local driving for structure growth.

This work was supported by the Deutsche Forschungsgemeinschaft.

REFERENCES

- [1] CROSS M. C. and HOHENBERG P. C., *Rev. Mod. Phys.*, **65** (1993) 851.
- [2] For a review see, *e.g.*, VAN SAARLOOS W., *Phys. Rep.*, **29** (2003) 386.
- [3] See, however, COULLET P. and KRAMER L., *Chaos*, **14** (2004) 244 for retracting fronts that appear in the presence of strongly nonlinear dispersion and that induce spatiotemporal intermittency.

- [4] POMEAU Y., *Physica D (Amsterdam)*, **23** (1986) 3.
- [5] BENSIMON D., SHRAIMAN D. I. and CROQUETTE V., *Phys. Rev. A*, **38** (1988) 5461.
- [6] LÜCKE M., BARTEN W., BÜCHEL P., FÜTTERER C., HOLLINGER ST. and JUNG CH., in *Evolution of Structures in Dissipative Continuous Systems*, edited by BUSSE F. H. and MÜLLER S. C., *Lect. Notes Phys.*, Vol. **m55** (Springer, Berlin) 1998, p. 127.
- [7] JUNG D., PhD Thesis (Universität des Saarlandes, Saarbrücken) 2005.
- [8] KOLODNER P., *Phys. Rev. E*, **50** (1994) 2731.
- [9] JUNG D., MATURA P. and LÜCKE M., *Eur. Phys. J. E*, **15** (2004) 293; MATURA P., JUNG D. and LÜCKE M., *Phys. Rev. Lett.*, **92** (2004) 254501.
- [10] BATISTE O. and KNOBLOCH E., *Phys. Rev. Lett.*, **95** (2005) 244501.
- [11] BATISTE O., KNOBLOCH E., ALONSO A. and MERCADER I., *J. Fluid Mech.*, **560** (2006) 149.
- [12] KOLODNER P., *Phys. Rev. E*, **48** (1993) R665; KOLODNER P., SLIMANI S., AUBRY N. and LIMA R., *Physica D (Amsterdam)*, **85** (1995) 165.
- [13] JUNG D. and LÜCKE M., *Phys. Rev. Lett.*, **89** (2002) 054502; *Phys. Rev. E*, **72** (2005) 026307.
- [14] SAKAGUCHI H. and BRAND H. R., *Physica D (Amsterdam)*, **97** (1996) 274.
- [15] COULLET P., RIERA C. and TRESSER C., *Phys. Rev. Lett.*, **84** (2000) 3069.
- [16] BURKE J. and KNOBLOCH E., *Phys. Rev. E*, **73** (2006) 056211.
- [17] BÜCHEL P. and LÜCKE M., *Phys. Rev. E*, **63** (2001) 016307.
- [18] RIECKE H., *Phys. Rev. Lett.*, **68** (1992) 301.